Journal of Magnetism and Magnetic Materials 322 (2010) 488–493

Contents lists available at ScienceDirect

Journal of Magnetism and Magnetic Materials

journal homepage: www.elsevier.com/locate/jmmm

Magnetization measurement of single $La_{0.67}Ca_{0.33}MnO_3$ nanotubes in perpendicular magnetic fields using a micromechanical torsional oscillator

D. Antonio *, M.I. Dolz [1], H. Pastoriza

Comisión Nacional de Energía Atómica, Centro Atómico Bariloche, (8400) S. C. de Bariloche, Argentina

ARTICLE INFO

Article history:
Received 27 May 2009
Received in revised form
24 September 2009
Available online 9 October 2009

PACS:
75.75.+ a
85.85.+ j
75.47.Lx

Keywords:
Micromachined magnetometers
Manganite nanotubes
Shape anisotropy

ABSTRACT

Using a silicon micromechanical resonator as a sensitive magnetometer, the authors have studied both experimentally and theoretically the magnetic behavior of two isolated ferromagnetic nanotubes of perovskite $La_{0.67}Ca_{0.33}MnO_3$. The article investigates the specific configuration where a magnetic field H is applied perpendicular to the magnetic easy axis of an isolated nanotube characterized by an uniaxial anisotropy constant K. In this situation, the magnetization M reduces the effective elastic constant k_M of the resonator. This softening of the mechanical system is opposed to the hardening effect of M observed in a previous work, where H was applied parallel to the easy axis. Moreover, in this magnetic field configuration two distinct magnetization regimes are manifested, depending on the magnitude of H. For $H \gg 2K/M$ the magnetization is almost parallel to the applied magnetic field and for $H \ll 2K/M$ it is almost parallel to the easy axis of the nanotube. At a certain value of H there is a sharp transition from one regime to the other, accompanied by a peak in the energy dissipation.

1. Introduction

If there once was "plenty of room at the bottom", today the world of nanoscience is brimful of interrelated disciplines, and nanomagnetism certainly occupies a large portion of that space [1]. This relevance in the field is bolstered by a large array of applications such as ultra-high density magnetic recording, spin electronics, and high-strength permanent magnets to name but a few. Among the broad variety of fabricated geometries, magnetic nanowires and nanotubes are an interesting result of nanopatterning, with emerging capabilities in future nano-electronic components [2,3], transducers or sensors [4,5], and solid-oxide fuel cells [6].

Manipulating and sensing these nanostructures is a challenging task which often requires the development of new tools and technologies. Recently, we have demonstrated that micromechanical torsional oscillators can be used to measure the magnetic properties of individual nanotubes [7]. These devices, fabricated with MEMS technology, extend all the advantages of high-Q mechanical oscillators [8] to the microscopic scale and serve as very sensitive micromagnetometers. To investigate these samples at low temperatures and with maximum sensitivity we have designed and integrated with the sensor a cryogenic CMOS transimpedance amplifier [9] that works down to a temperature of 4 K. The result is a micromagnetometer that allows detection of magnetic moments as small as 10^{-11} emu.

In this work, we study the magnetic properties of ferromagnetic nanotubes of perovskite $La_{0.67}Ca_{0.33}MnO_3$ in the particular configuration where the magnetic field is applied perpendicular to the magnetic easy axis. In this configuration the applied and anisotropy fields favor different and competing magnetization directions. Experimentally, we observe a negative non-monotonic resonant frequency variation in the microresonator. Our purpose is to explain this response, confirming the micromechanical resonator as a suitable instrument for the measurement of magnetic properties at the nanoscale. To this end, we propose a simple model for the nanotube's magnetic energy that relates the frequency variations with the nanotube's magnetic moment. We then call attention to the manifestation of two distinct magnetization regimes depending on the magnitude of the applied magnetic field. For low fields the magnetization is parallel to the easy axis, and it is parallel to H for high fields. Finally, we discuss how these two regimes are separated by a sharp transition which is coincident with a peak of energy dissipation in the system, denoted by a minimum in the quality factor of the mechanical resonator.

2. Measuring ferromagnetic samples with the microresonator

The polysilicon mechanical microresonator was fabricated in the MEMSCAP [10] foundry using its multiuser process (MUMPS).

* Corresponding author. Tel.: +54 2944 445171; fax: +54 2944 445299.
E-mail address: dario.antonio@cab.cnea.gov.ar (D. Antonio).
[1] Present address: Departamento de Física, Universidad Nacional de San Luis, (5700) San Luis, Argentina.

0304-8853/$ - see front matter © 2009 Elsevier B.V. All rights reserved.
doi:10.1016/j.jmmm.2009.10.002

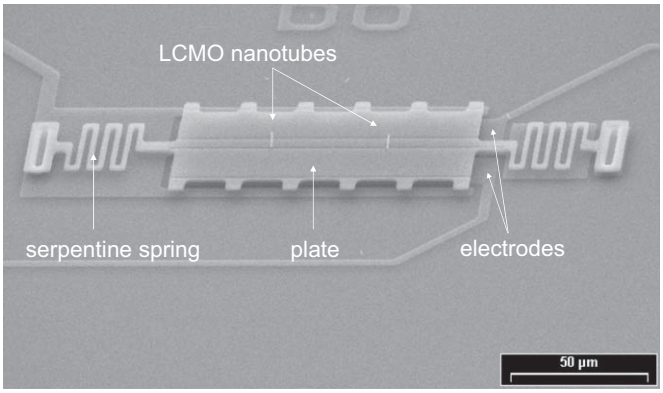

Fig. 1. High-Q silicon microresonator with the two attached LCMO nanotubes. The separation between nanotubes is 40 μm and their magnetic easy axis is perpendicular to the oscillator's rotation axis.

The structure consists of a suspended central plate that is anchored to the substrate by means of two serpentine springs, and electrically grounded. This plate is harmonically driven by a 100 mV peak-to-peak ac voltage applied in one underlying electrode, and its motion is detected through the capacitance variation in the other electrode (see Fig. 1). The natural resonant frequency v_0 of the oscillator's torsional mode is given by

$$v_0 = \frac{1}{2\pi}\sqrt{\frac{k_e}{I}} \tag{1}$$

where I is the moment of inertia and k_e is the elastic constant of the oscillator. For this particular resonator $v_0 \approx 72$ kHz. When a magnetic sample is attached to the plate of the oscillator, and an external magnetic field is applied, the magnetic interaction between the sample and the applied field produces a variation k_M in the effective elastic constant [11]. As a result the resonant frequency changes to

$$v_r = \frac{1}{2\pi}\sqrt{\frac{k_e + k_M}{I}} \tag{2}$$

Considering $k_M \ll k_e$, and with $\Delta v = v_r - v_0$, k_M is given by

$$k_M \approx 8\pi^2 I v_0 \Delta v \tag{3}$$

The microresonator has a high quality factor $Q \approx 10^5$ at low temperatures, which is substantial for the high sensitivity of the device. Furthermore, when the resonator is harmonically driven the amplitude of the resonance depends on Q and provides information about the sample's dissipative processes that draw energy from the mechanical system.

3. Theory

3.1. Magnetic energy

An outline of the system studied is shown in Fig. 2. The angles used are measured from the direction perpendicular to the easy axis of magnetization, θ representing the direction of the applied magnetic field H and φ the direction of the magnetization M.

Assuming uniaxial anisotropy, the magnetic energy of the system is given by

$$\frac{E}{V} = -MH\cos(\varphi - \theta) + K\sin\left(\frac{\pi}{2} - \varphi\right)^2 \tag{4}$$

where V is the volume of the magnetic sample and K is the anisotropy constant.

The first term of the equation represents the potential energy of a magnet in an applied field and is minimized when the magnetization is parallel to this field. The second term is associated with the demagnetizing field of the sample. It is minimized when the magnetization is parallel to the easy axis. When the applied field is not aligned with the easy axis, these two energies are competing. Indeed, we shall see that if the field is small ($H \ll 2K/M$), the anisotropy wins and the magnetization is in the direction of the easy axis. Conversely, at high fields ($H \gg 2K/M$) the torque exerted by H overcomes the anisotropy and the magnetization is parallel to the applied magnetic field [12]. For intermediate values of H the magnetization will be in between these two directions and the angle φ will be such that the total energy is minimized. In order to find the angle φ_{eq} corresponding to the equilibrium magnetization we need to take the first derivative of the energy with respect to φ and set it equal to zero. When $\theta \ll 1$ this calculation results in the following equation:

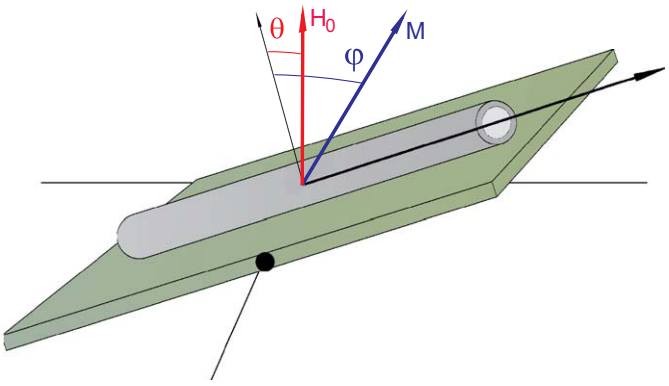

Fig. 2. Diagram of the magnitudes, directions and angles used in the experiment.

$$\tan(\varphi_{eq}) - \theta - \frac{2K}{MH}\sin(\varphi_{eq}) = 0 \tag{5}$$

This equation can be solved numerically as will be shown later, but an approximate solution can be found analytically for both low and high fields.

3.2. Magnetization angle

3.2.1. High fields $H \gg 2K/M$

If $H \gg 2K/M$, and assuming $\theta \ll 1$, the magnetization will become almost parallel to the applied field ($\varphi_{eq} \approx \theta$). Eq. (5) can then be simplified to

$$\varphi_{eq} - \theta - \frac{2K}{MH}\varphi_{eq} = 0 \tag{6}$$

which leads to

$$\varphi_{eq} \approx \frac{\theta}{1 - \frac{2K}{MH}} \tag{7}$$

3.2.2. Low fields $H \ll 2K/M$

If $H \ll 2K/M$, the magnetization will be almost in the direction of the easy axis ($\varphi_{eq} \approx \pi/2$) and Eq. (5) can be simplified to

$$-\frac{1}{\varphi_{eq} - \frac{\pi}{2}} - \theta - \frac{2K}{MH} = 0 \tag{8}$$

which gives for $\theta \ll 1$

$$\varphi_{eq} \approx \frac{\pi}{2} - \frac{H}{\frac{2K}{M}} \tag{9}$$

3.3. Effective elastic constant

According to Eq. (4) the magnetic energy depends on θ in such a way to introduce a variation k_M in the effective elastic constant of the resonator-nanotube system. This in turn induces a change in the oscillator resonant frequency Δv given by Eq. (3). The value of k_M can be evaluated by taking the second derivative of the magnetic energy with respect to θ. This can be done for both the high and low field approximations after replacing φ in Eq. (4) by the values of φ_{eq} given by Eqs. (7) and (9) respectively. In this calculation we consider $\theta = \theta_0 + \theta_r$ where $\theta_0 \ll 1$ is a constant angle representing the minor initial misalignment between H and the direction perpendicular to the easy axis, and θ_r is the actual oscillating angle.

First, for the high field approximation we assume that the magnetization is saturated and $M = M_S$, where M_S is the saturation magnetization. This gives

$$\Delta v \approx \frac{V}{8\pi^2 I v_0}\frac{2KM_SH}{(2K - M_SH)} \tag{10}$$

Next, in the low field approximation where M is certainly not saturated we can suppose a linear dependence with H of the form $M \approx M_0 + \chi H$. Here M_0 is the initial magnetization for $H = 0$ and χ is the low field susceptibility. With these considerations, the variation of the resonant frequency at low fields can be approximated by

$$\Delta v \approx \frac{1}{8\pi^2 I v_0}\left(M_0\theta_0 H + \left(\frac{M_0^2}{2K} - 2\chi\right)H^2\right) \tag{11}$$

4. Experimental

A powder of nanotubes was fabricated by the pore-filling method in a holed plastic template, starting from a liquid solution of $La(NO_3)_{3.6}H_2O$, $Ca(NO_3)_{2.4}H_2O$, and $Mn(NO_3)_{2.4}H_2O$, followed by denitration and calcination steps [13]. From this powder, two nanotubes with a diameter of 700 nm and a length of 9.5 μm were chosen using a scanning electron microscope. They then were placed on top of the oscillator's plate using hydraulic micro-manipulators under an optical microscope, and glued to it with a sub-micrometer drop of Apiezon N© grease. The microresonator with the attached nanotubes was inserted into an ^{4}He cryostat equipped with a 4 T magnet.

In this experiment we used for the first time in a practical application our recently developed cryogenic transimpedance amplifier [9] which was connected and adjacent to the micro-resonator, inside the cryostat. This lead to a considerable reduction of noise in the detected signal, compared to our previous measurements of isolated nanotubes [7]. In addition, the amelioration of the measured signal allowed us to implement a closed loop configuration which is outlined in Fig. 3. The resulting sensitivity was two orders of magnitude higher than in the setup using open-loop excitation and conventional electronics.

The microresonator was actuated electrostatically by means of an HP 3324A function generator which has a resolution of 1 mHz. The movement of the microresonator was sensed capacitively with the cryogenic transimpedance amplifier. In this way, the signal was preamplified at low temperatures and then input into a digital EG&G 5302 lockin amplifier at room temperature. Then a computer connected with the lockin via an GPIB interface read the amplitude and phase of the signal. Finally a PID program changed the frequency of excitation in order to keep the microresonator in the resonance.

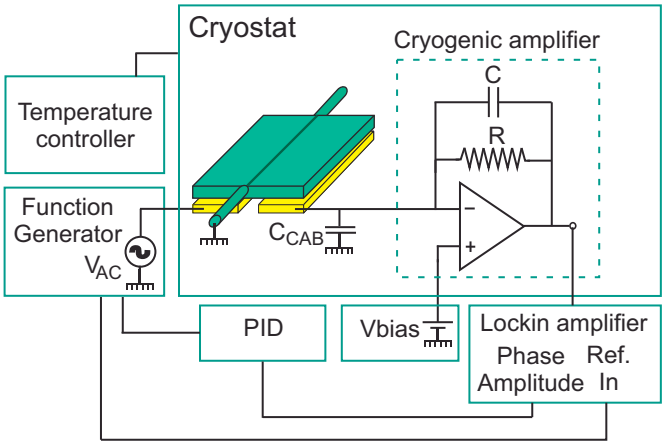

Fig. 3. Experimental setup. The oscillator's motion is sensed and preamplified by the cryogenic amplifier inside the dewar and then amplified by the lockin amplifier at room temperature. This signal is used to control the frequency of excitation in order to keep the oscillator at the resonance.

5. Results and discussion

5.1. Measurement of the resonant frequency variation

The variation of the resonant frequency Δv is directly related to k_M by Eq. (3). The measurements of Δv at different temperatures and as a function of the applied magnetic field are presented in Fig. 4. Additionally, in this figure we have included one curve from a previous work where the field was applied parallel to the magnetic easy axis. In that case, the frequency variation was always positive and monotonic since both the applied field and the anisotropy forced the magnetization in the same direction. In contrast, when the field is applied perpendicular to the easy axis the frequency variation is negative and non-monotonic. Two different regimes separated by a minimum in the value of Δv can be clearly identified. As will be shown later the first part of the curve corresponds to the low field regime, where the magnetization is almost in the direction of the easy axis. The second part of the curve corresponds to the high field regime, in which the magnetization points in the direction of the applied magnetic field.

5.2. Determination of K and M_S from the high field approximation

In the high field regime Eq. (10) can be used to extract some quantitative parameters. However, it is more convenient to invert both terms of this equation [7], which gives

$$\frac{1}{\Delta v} \approx \frac{8\pi^2 I v_0}{V}\left(\frac{1}{M_SH} - \frac{1}{2K}\right) \tag{12}$$

But before proceeding to the extraction of the parameters it is important to point out that Eq. (12) is valid for a ferromagnetic response with a saturated magnetization, which in these nanotubes is valid only up to a field $H \approx 10$ KOe. In effect, it has been shown [14] that the nanoparticles constituting the wall of these nanotubes have a shell with a thickness of approximately 2 nm which is non-ferromagnetic. This shell with crystalline disorder is formed by small ferromagnetic clusters that interact with each other antiferromagnetically. For low fields this shell does not contribute to the magnetic response of the nanotubes and is thus considered as a "magnetically dead layer". But for fields higher than 10 KOe the antiferromagnetic interactions in this layer are modified, resulting in a contribution to the total magnetic response that can be associated with a high field

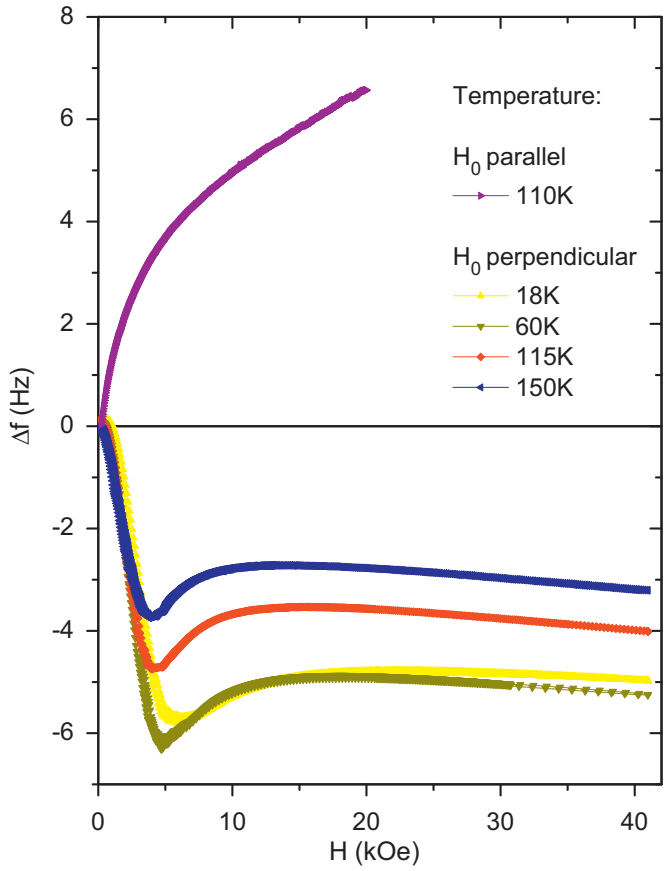

Fig. 4. Variation of the oscillator's resonant frequency as a function of the applied magnetic field. In the case of an applied field parallel to the easy magnetic axis the variation is always positive and monotonic. In the case of an applied field perpendicular to the easy magnetic axis the frequency variation is always negative and non-monotonic.

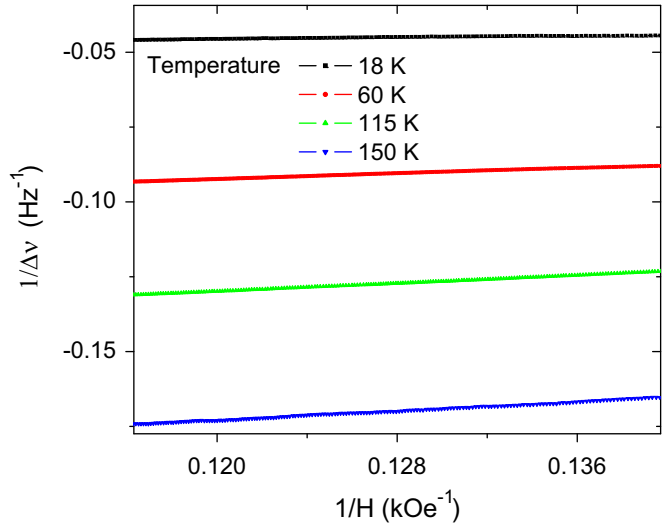

Fig. 5. Reciprocal of the resonant frequency variation as a function of $1/H$. Applying a linear fit to $1/\Delta\nu$ vs. $1/H$ at high fields we could extract M_S and K from the slope and the intercept values respectively.

susceptibility. In consequence, to extract the parameters of Eq. (12) we must use the data corresponding to the field range where the magnetization is saturated but the magnetic dead layer does not yet contribute to the total magnetic response. The $1/\Delta\nu$ vs. $1/H$ curve is shown in Fig. 5 for this field range. From the linear square fit of these curves we can then obtain the values of K and

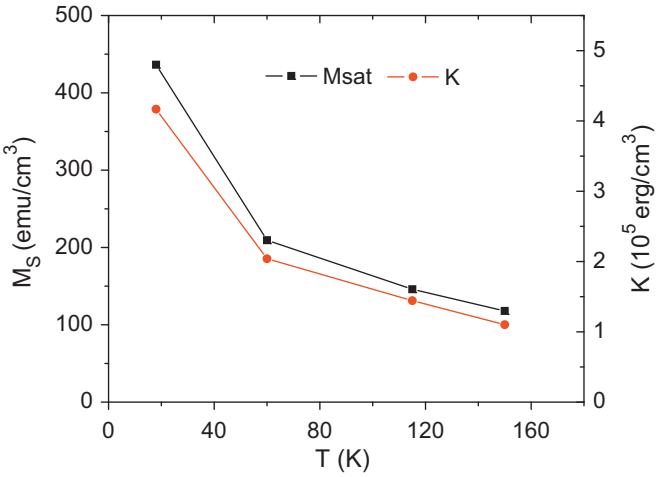

Fig. 6. Values of K and M_S obtained from the linear fit of the $1/\Delta\nu$ vs. $1/H$ curve at high fields.

M_S, which are shown in Fig. 6. It is clear from the figure that the anisotropy energy does not follow the expected dependence for the shape anisotropy of an homogeneous ellipsoid ($K \propto M^2$). The non-uniformity of the demagnetization field in this tubular geometry and the granular morphology of the nanotubes could account for this effect.

5.3. Determination of χ from the low field approximation

On the other hand, at the low field range more information can be obtained about the magnetic properties of the nanotubes. It can be seen from Eq. (11) that applying a polynomial fit to the measured $\Delta\nu$, with H as the independent variable, we could obtain the value of M_0 and χ from linear (P_1) and quadratic (P_2) terms respectively. However, the linear term is proportional to θ_0 which is small and has a large error. Nevertheless if $M_0 < 100\,\mathrm{emu/cm^3}$, and with the obtained values for $P_2 \approx -0.16$, then P_2 depends almost exclusively on χ, and:

$$\Delta\nu \approx \frac{1}{8\pi^2 I\nu_0}(M_0\theta_0 H - 2\chi H^2) = P_0 + P_1 H + P_2 H^2 \tag{13}$$

This is the case for the curve corresponding to a temperature $T = 150\,\mathrm{K}$ which was used to obtain a representative value of χ. The detail of this curve for low magnetic fields is shown in Fig. 7 where the parabolic behavior can be identified. From the second order polynomial fit of this curve and using Eq. (13) we obtained $\chi \approx 0.07\ \mathrm{emu/(cm^3\,Oe)}$.

5.4. Magnetization angle in the full magnetic field range

With the values obtained previously for K, M_S, and χ, it is possible to solve numerically Eq. (5) in order to find the value of φ_{eq} for all the values of H. But before doing this it is necessary to establish an expression for the amplitude of the magnetization. This value is $M = M_0 + \chi H \sin(\theta)$ when the magnetization is parallel to the easy axis (low fields). As the magnetic field rises, the magnetization angle rotates towards the direction of the applied field. The component of the magnetization parallel to the easy axis is still given by $M_0 + \chi H \sin(\theta)$ but an additional component appears in the direction of the field such that the total magnetization is at an angle φ with H. From simple geometry the total magnetization is then $M = \chi\ \sin(\theta)H/\sin(\varphi)$. This is true up to the magnetic field where $M = M_S$, which is the maximum value for M at that temperature. As H continues to increase from this value, M continues to rotate towards the direction of the magnetic field but with a constant amplitude

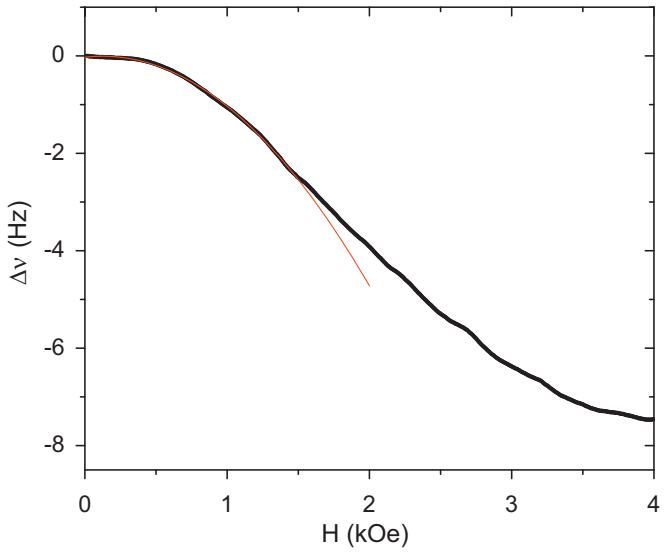

Fig. 7. Oscillator's resonant frequency variation for low fields and for $T = 150$ K. The low field susceptibility χ was evaluated from the second order polynomial fit of the curve (shown in red in the figure). (For interpretation of the references to color in this figure legend, the reader is referred to the web version of this article.)

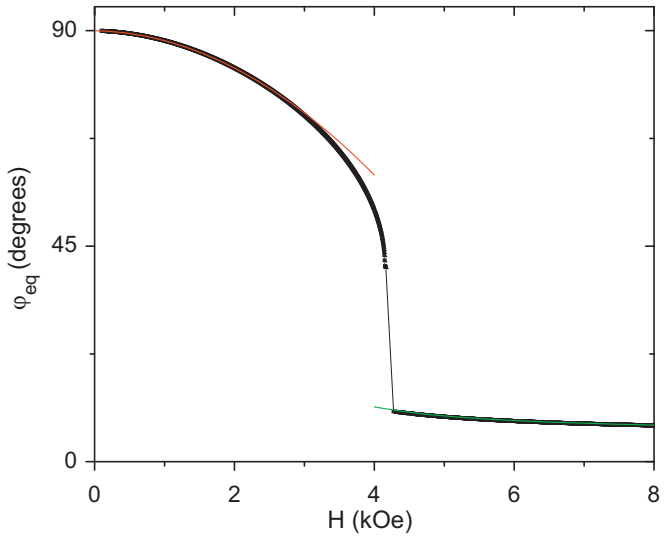

Fig. 8. Magnetization angle as a function of the applied magnetic field. This value was obtained by numerically solving the equation for the magnetic energy with the values of M_S, K, and χ extracted from the measurements of $\Delta\nu$. At low fields the magnetization is almost aligned with the magnetic easy axis. At high fields the magnetization is almost aligned with the magnetic field. The analytical solutions to the high and low field approximations are shown in green and red respectively. (For interpretation of the references to color in this figure legend, the reader is referred to the web version of this article.)

$M = M_S$. This dependence of M with H was considered when solving Eq. (5), and the solution for φ_{eq} is plotted in Fig. 8. Additionally the curves corresponding to the approximation of φ at high fields, given by Eq. (7), and at low fields, given by Eq. (9), are plotted in the same figure. It is clear from this figure that for low fields the magnetization points in the direction of the easy axis. As the field rises the magnetization starts rotating towards the direction of the applied field and at a certain value of H there is a sharp decrease in φ_{eq} which means that M gets aligned with the applied field. This sudden change in the magnetization occurs for an applied magnetic field $H_p \approx 0.4$ T for $T = 150$ K. Getting back to the curve for $T = 150$ K in Fig. 4 we can see that this value of H corresponds to the minimum value of $\Delta\nu$. This point marks the limit between the low and the high field regimes.

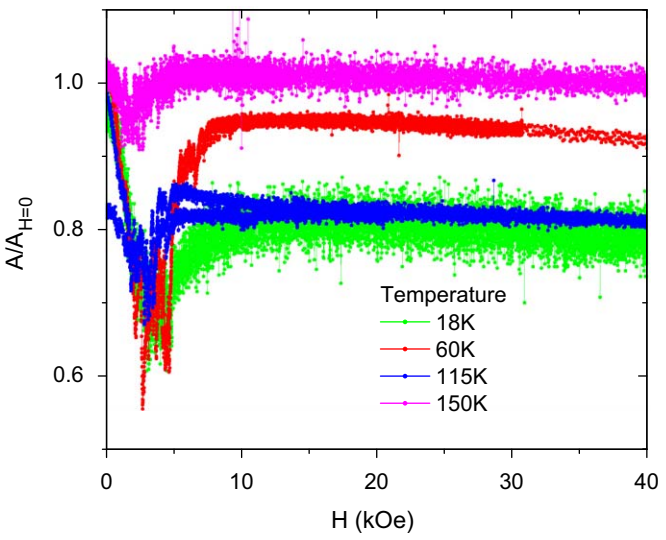

Fig. 9. Amplitude of the resonance as a function of the applied magnetic field, normalized by the amplitude of the resonance at $H = 0$.

5.5. Dissipation

The amplitude of the voltage signal detected by the lockin amplifier is proportional to the amplitude of the mechanical oscillations. At the resonance this magnitude is proportional to the quality factor of the resonator, and consequently it is inversely proportional to the dissipated energy. Therefore, a decrease in the detected voltage implies that more energy is necessary to keep the plate oscillating with the same amplitude. In Fig. 9 the resonance amplitude A is shown as a function of H for different temperatures, normalized by the value of A at $H = 0$. It can be seen that in all the curves there is a clear increase of the energy dissipation at H_p. This can be explained by the fact that at the vicinity of this point small variations of H induce large changes in M. In fact, as the plate oscillates, the field that is effectively applied to the nanotube rotates. This produces a periodic variation of the magnetization, which is much larger for $H \approx H_p$ than for the rest of the applied field range. Therefore, in each oscillating period a minor hysteresis loop is produced, and the area of this loop peaks for $H \approx H_p$. Consequently, at this field the energy absorbed by the magnetic system is maximum. It was proposed that a second order phase transition as a function of magnetic field is occurring in this configuration [12]. The dissipation observed in our experiment can be correlated with the fluctuations associated with this transition.

6. Conclusion

In this work the micromechanical resonator was confirmed as a suitable tool for measuring magnetic properties at the nanoscale. We studied two isolated nanotubes of perovskite $La_{0.67}Ca_{0.33}MnO_3$ with an external magnetic field H applied perpendicular to the magnetic easy axis. In this configuration the anisotropy energy and the applied field potential energy were competing, and a negative non monotonic frequency variation was measured as a function of applied field. At the applied field H_p, corresponding to the minimum frequency variation, a peak in the energy dissipation was detected.

In order to explain this behavior we extracted the saturation magnetization, the anisotropy constant, and the low field susceptibility from the resonance curves. With these magnitudes we solved numerically the equation for the magnetization angle and found that H_p marks the limit between two distinct regimes.

For applied fields lower than H_p the magnetization is almost parallel to the easy axis and for fields higher than H_p the magnetization is almost parallel to the applied field. The transition between these regimes is abrupt and the peak of energy dissipation is a consequence of this. In fact, as the nanotube oscillates the effective applied field varies periodically, producing minor magnetization hysteresis loops. When $H \approx H_p$ the variation of the magnetization in each cycle is much larger than for the rest of the applied field range. This represents larger hysteresis loops and consequently a peak in the energy dissipation.

Acknowledgments

We would like to thank A.G. Leyva for providing the samples and W. Bast for mounting the nanotubes.

We wish to acknowledge the support of ANPCyT, Argentina, through Grants PAE 2004-22592 and PICT04-21372; and U.N. Cuyo through Grant 06/C258.

References

[1] R. Skomski, Nanomagnetics, J. Phys. Condens. Matter 15 (2003) R841–R896.
[2] H.W.C. Postma, T. Teepen, Z. Yao, M. Grifoni, C. Dekker, Carbon nanotube single-electron transistors at room temperature, Science 293 (2001) 76–79.
[3] A. Bachtold, P. Hadley, T. Nakanishi, C. Dekker, Logic circuits with carbon nanotube transistors, Science 294 (2001) 1317–1320.
[4] L. Hueso, N. Mathur, Dreams of a hollow future, Nature 427 (2004) 301–304.
[5] E. Comini, G. Faglia, G. Sberveglieri, Z. Pan, Z.L. Wang, Stable and highly sensitive gas sensors based on semiconducting oxide nanobelts, Appl. Phys. Lett. 81 (2002) 1869.
[6] A.G. Leyva, J. Curiale, H. Troiani, M. Rosenbusch, P. Levy, R.D. Sanchez, Nanoparticles of $La_{(1-x)}Sr_xMnO_3$ ($x = 0.33, 0.20$) assembled into hollow nanostructures for solid oxide fuel cells, Adv. Sci. Technol. 51 (2006) 54–59.
[7] M.I. Dolz, W. Bast, D. Antonio, H. Pastoriza, J. Curiale, R.D. Sánchez, A.G. Leyva, Magnetic behavior of single $La_{0.67}Ca_{0.33}MnO_3$ nanotubes: surface and shape effects, J. Appl. Phys. 103 (2008) 083909.
[8] R.N. Kleiman, G.K. Kaminsky, J.D. Reppy, R. Pindak, D.J. Bishop, Single-crystal silicon high-Q torsional oscillators, Rev. Sci. Instrum. 56 (1985) 2088.
[9] D. Antonio, H. Pastoriza, P. Julián, P. Mandolesi, Cryogenic transimpedance amplifier for micromechanical capacitive sensors, Rev. Sci. Instrum. 79 (2008) 084703.
[10] Memscap Inc., 4021 Stirrup Creek Drive, Durham, NC 27703 〈http://www.memscap.com〉.
[11] M. Dolz, D. Antonio, H. Pastoriza, Measurement of mesoscopic high-Tc superconductors using Si mechanical micro-oscillators, Physica B 398 (2007) 329–332.
[12] P. Vargas, D. Laroze, Thermodynamics of three-dimensional magnetic nanoparticles, J. Magn. Magn. Mater. 272–276 (2004) e1345–e1346.
[13] A.G. Leyva, P. Stoliar, M. Rosenbusch, V. Lorenzo, P. Levy, C. Albonetti, M. Cavallini, F. Biscarini, H. Troiani, J. Curiale, R.D. Sanchez, Microwave assisted synthesis of manganese mixed oxide nanostructures using plastic templates, J. Solid State Chem. 177 (2004) 3949–3953.
[14] J. Curiale, M. Granada, H.E. Troiani, R.D. Sánchez, A.G. Leyva, P. Levy, K. Samwer, Magnetic dead layer in ferromagnetic manganite nanoparticles, Appl. Phys. Lett. 95 (2009) 043106.